PERGAMON

Journal of Structural Geology 23 (2001) 979–989

JOURNAL OF STRUCTURAL GEOLOGY

www.elsevier.nl/locate/jstrugeo

A sensitive vorticity gauge using rotated porphyroblasts, and its application to rocks adjacent to the Alpine Fault, New Zealand

Rodney J. Holcombe[a,*], Timothy A. Little[b]

[a]*Department of Earth Sciences, The University of Queensland, Qld 4072, Australia*
[b]*School of Earth Sciences, Victoria University of Wellington, P.O. Box 600, Wellington, New Zealand*

Received 4 February 1999; accepted 14 January 2000

Abstract

Variable aspect ratio porphyroblasts deformed in non-coaxial flow, and internally containing rotated relicts of an external foliation, can be used to characterise plane strain flow regimes. The distribution obtained by plotting the orientation of the long axis of such grains, classified by aspect ratio, against the orientation of the internal foliation is potentially a sensitive gauge of both the bulk shear strain (as previously suggested) and kinematic vorticity number.

We illustrate the method using rotated biotite porphyroblasts in the Alpine Schist, a sequence of mid-crustal rocks that have been ramped to the surface along the Alpine Fault, a major transpressional plate boundary. Results indicate that, at distances $\geq\sim$1 km from the fault, the rocks have undergone a combination of irrotational flattening and dextral-oblique, normal-sense shear, with a bulk shear strain of $\sim$0.6 and kinematic vorticity number of $\sim$0.2. The vorticity analysis is compatible with estimates of strongly oblate bulk strain of $\sim$75% maximum shortening. Dextral-reverse transpressional flow characterises higher strain S-tectonite mylonite within $\sim$1 km of the Alpine Fault. These relationships provide insight into the kinematics of flow and distribution of strain in the hangingwall of the Alpine Fault and place constraints on numerical mechanical models for the exhumation of these mid-crustal rocks.

1. Introduction

Rigid objects embedded in a viscous medium undergoing general non-coaxial flow will tend to rotate with respect to the bulk kinematic framework. The theory of such flow behaviour for two-dimensional monoclinic (plane-strain) flow systems is now reasonably well documented (e.g., Ghosh and Ramberg, 1976; Passchier, 1987), although the extension of such theory to three dimensions and triclinic systems may be fraught with difficulty (Robin and Cruden, 1994; Tikoff and Fossen, 1995; Jiang and Williams, 1998; Lin et al., 1998). The theory is most straightforward for steady-state monoclinic flow systems that can be modelled as a combination of simultaneous pure and simple shear strain histories where the shear direction is parallel to an instantaneous principal stretch of the pure shear component. Ghosh and Ramberg (1976) used the ratio of pure to simple shear rate to characterise the degree of non-coaxiality of plane strain, sub-simple shear flow (in this kinematic framework). The kinematic vorticity number, W_k (Lister and Williams, 1983; Passchier, 1987; Means, 1994) is a numerically related measure, based on the ratio of the rate of internal rotation (vorticity) to the rate of stretching strain. Pure shear flow has a vorticity number of zero, simple shear flow has a vorticity number of one, and most general flow regimes fall between 0 and 1.

Passchier and Trouw (1996) summarise a number of proposed vorticity gauges. For example, Passchier (1987) used the property that, in any general shear, rigid porphyroclasts whose shape is above a specific axial ratio can become stationary at high strain as they rotate into the asymptotic flow apophyses. His application of the method involved defining the aspect ratio cut-off value below which no stable orientations exist, such cut-off values being a measure of the vorticity number. The method relied on strain being high enough for enough porphyroclasts to reach stable orientations in order to statistically define the cut-off value. Ghosh (1987) showed how W_k can be calculated for steady-state monoclinic flow from the actual rotation of a spherical object (or from the bulk shear strain, γ) if both the actual rotation of the object (or γ) and the finite principal stretches are known. Such rotations are cited for equant (sub-spherical) syntectonic porphyroblasts (e.g, garnet) that contain rotated elements of the external shear fabric.

In this paper, we present the theory for a technique for measuring kinematic vorticity number in sub-simple shear

* Corresponding author. Fax: +61-7-3365-1277.
E-mail address: rodh@earthsciences.uq.edu.au (R.J. Holcombe).

0191-8141/01/$ - see front matter
PII: S0191-8141(00)00169-3

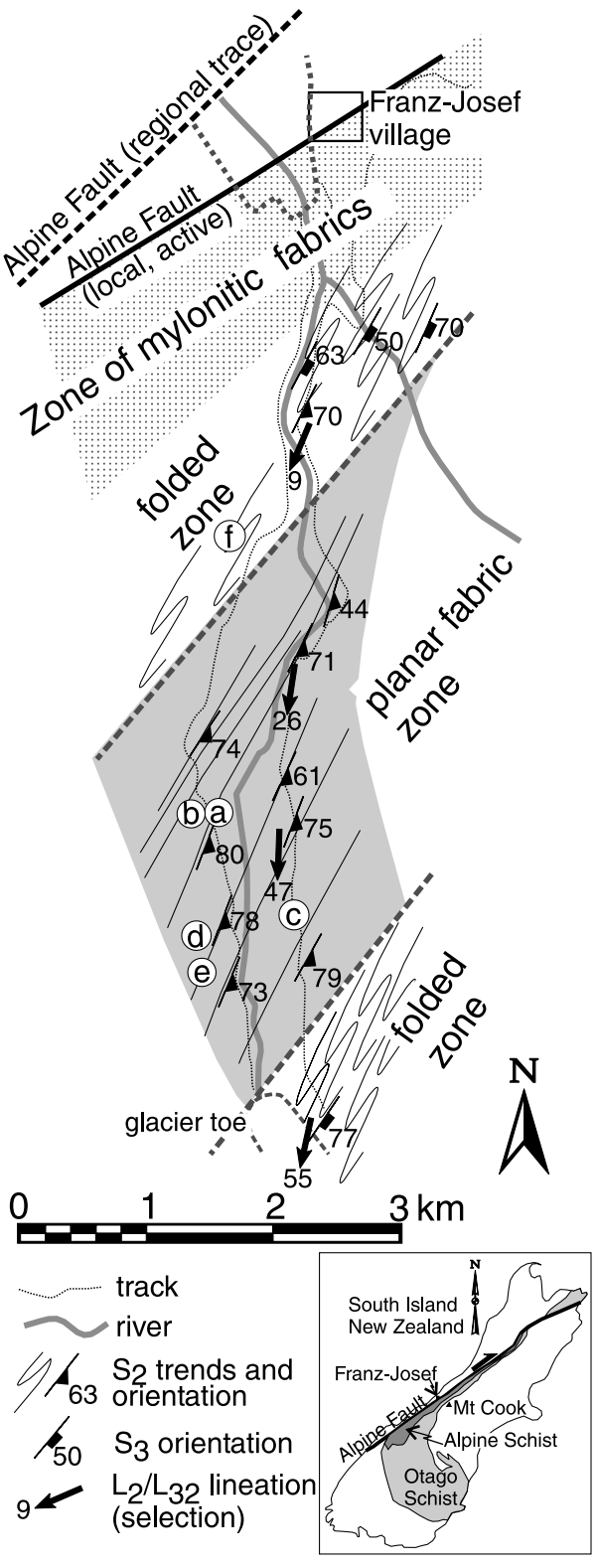

Fig. 1. Location and general structure of the Alpine Schist adjacent to the Alpine Fault near Franz Josef, New Zealand, showing the major structural domains. Circles labelled *a–f* mark the location of samples used in the vorticity analyses of Fig. 6. A strong composite lineation on the S_2 surface (L_2) and the S_2/S_3 intersection lineation are colinear and both steepen systematically away from the Alpine Fault.

flow that uses elements of the methods of both Ghosh (1987) and Passchier (1987). We apply the method to characterise flow in the hangingwall of the Alpine Fault in the South Island of New Zealand, an active obliquely convergent plate margin in which plate motion remains oblique, rather than being spatially partitioned into distinct zones of strike-slip and convergent deformation (Norris et al., 1990).

Initiated in the Early Miocene as a dextral strike-slip transform fault (Cooper et al., 1987; Sutherland, 1995), since ~6.4 Ma, the Pacific Plate has converged obliquely into the Australian Plate at ~20°, resulting in ~90 km of shortening and ~230 km of dextral strike-slip (Walcott, 1998). The bulk of this transpressional deformation has been absorbed by delamination of the Pacific Plate at mid-crustal depths (Wellman, 1979) and by slip on the Alpine fault and shear in its adjacent ~1-km-thick mylonite zone (Norris and Cooper, 1995, 1997). At least some motion, however, is accommodated by distributed deformation of Pacific Plate rocks to the east as these rocks are ramped upward and tilted to the southeast above the footwall of the ~50° southeast-dipping Alpine Fault. The deepest exposed levels of the Pacific Plate hangingwall rocks along the Alpine Fault consist of a relatively narrow (12–25 km) band of amphibolite- to greenschist-facies rocks that are referred to as the Alpine Schist (Fig. 1).

Dextral-reverse slip on the southeast-dipping Alpine Fault, coupled with rapid erosion, has resulted in uplift and exhumation of this mid-crustal sequence from depths of 20–30 km during the past ~3–5 my (Holm et al., 1989; Norris et al., 1990; Grapes and Watanabe, 1992). Metamorphic isograds strike subparallel to the Alpine Fault and increase in grade toward the fault (Grapes, 1995), but are deformed by the final stages of ductile deformation in the schist. We infer that late increments of ductile deformation in the Alpine Schist are related to late Cenozoic uplift of these rocks on the Alpine Fault, and that these fabrics have been frozen-in during uplift and cooling of the rocks through the brittle–ductile transition zone (Holm et al., 1989).

Porphyroblast-rich fabrics in the compositionally uniform metapelitic units of the Alpine Schist provide a potential record of the kinematics of flow at depth within a currently active zone of oblique plate convergence. Individual biotite porphyroblasts commonly overgrow multiple distinctive graphitic laminae in the schist such that each internal lamination can easily be correlated with its external parent. Thus, we have fine-scale displacement and rotation gauges in these rocks that can be used to determine the flow kinematics as well as elements of the accumulated finite strain following porphyroblast growth.

2. A vorticity gauge based on rotated inequant porphyroblasts

In a non-coaxial flow, porphyroblasts that have overgrown

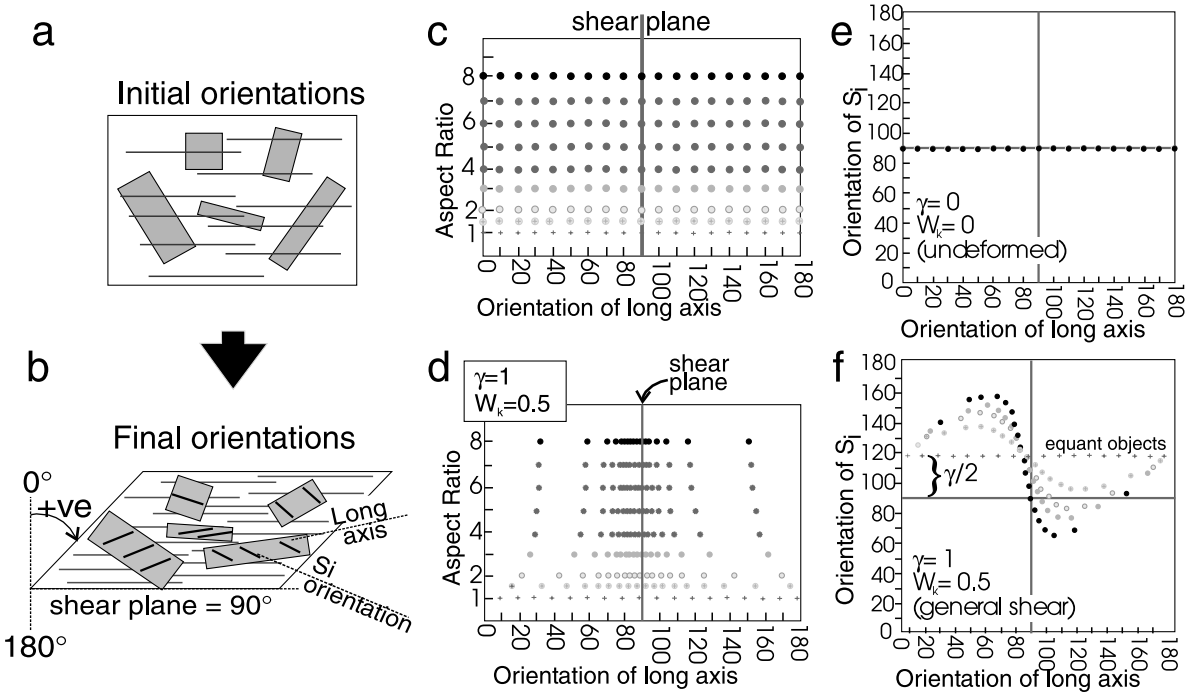

Fig. 2. Initial and final orientation distributions of rotated porphyroblasts that have overgrown a fabric parallel to the shear plane. Initial (undeformed) configurations are shown in the top figures, final (deformed) in the lower figures. All orientations and angles are in degrees. (a,b) Illustration of scenario, and definition of terms and angle conventions. The zero angle is normal to the shear plane, the direction of shear is positive, and the shear plane in the shear direction is 90°. Orientation angles are constrained to the range 0–180°; (c,d) distribution of long axes of objects of specified aspect ratio with initial uniform orientation distribution. Objects of aspect ratios of eight behave effectively as objects of infinitely large aspect ratio. (e,f) Orientation distribution of long axes plotted against orientation of S_i (LA/S_i plots) for the initial uniform distribution shown in (c) (see text for discussion). The greyscale of the points corresponds to the aspect ratios in (c) and (d). The curve for aspect ratios of eight is effectively the theoretical limit of the distribution.

the external shear fabric may contain a rotated relict of that fabric as an internal foliation. In rigid porphyroblasts the degree of rotation can be measured directly (Fig. 2a and b) from the orientation of the internal fabric relative to its matrix orientation (provided that these can be correlated). For steady-state monoclinic deformation the amount of rotation is a function of the bulk shear strain, γ, parallel to the shear direction, and the vorticity number, W_k, as well as on the initial orientation of the porphyroblast long axis relative to the shear direction (see Fig. 2b for angle and sign conventions used). The final orientation of any given initial porphyroblast can be calculated from the established relationships (Ghosh and Ramberg, 1976; Ghosh, 1987) and theoretical orientation distributions can be modelled for given initial distributions.

Critical to this model is the requirement that the angular difference between the internal and external foliations within the porphyroblasts reflects true synkinematic rotation. Preservation of inherited foliations within porphyroblasts, oblique to the external foliation, are common in multiple deformed rocks, arising, for example, from overgrowth of crenulations. Thus, the internal foliation must be correlated specifically with the external foliation before using the relative orientations as a rotation gauge.

Long axis orientation versus aspect ratio plots (Fig. 2c and d) contain elements that may enable W_k of a steady-state monoclinic flow to be determined, provided the entire distribution can be recognised (e.g. Passchier, 1987). However, provided that the S_i orientation reflects the rigid body rotation as discussed above, much more kinematic information is contained within plots of the orientation of the long axis of each porphyroblast versus the orientation of its internal foliation, S_i (LA/S_i plots, Fig. 2e and f). In these plots, orientation angles (constrained to a 0–180° range) are relative to the normal shear plane, with the direction of shear being positive, and the shear plane being 90° (Fig. 2b). The initial orientation of S_i of all porphyroblasts, irrespective of aspect ratio, is parallel to the shear plane (90°) and thus the initial distribution of all porphyroblasts in an LA/S_i plot lies on a single horizontal line through the centre of the plot. On deformation, this single line distribution splits into a series of asymmetric curves for each aspect ratio.

The precise pattern of the distribution curves in an LA/S_i plot is unique for any combination of bulk shear (γ) and vorticity number (W_k). In pure shear flow (zero shear strain rate) all the curves pass through the intersection of the 90° axes (Fig. 3b) which is also a centre of symmetry. The 'peakedness' of the pure shear curves is then a function of the finite strain (ellipticity of the strain ellipse). For simple shear flow all porphyroblasts rotate with a single sense of rotation and hence all curves lie above the horizontal 90°

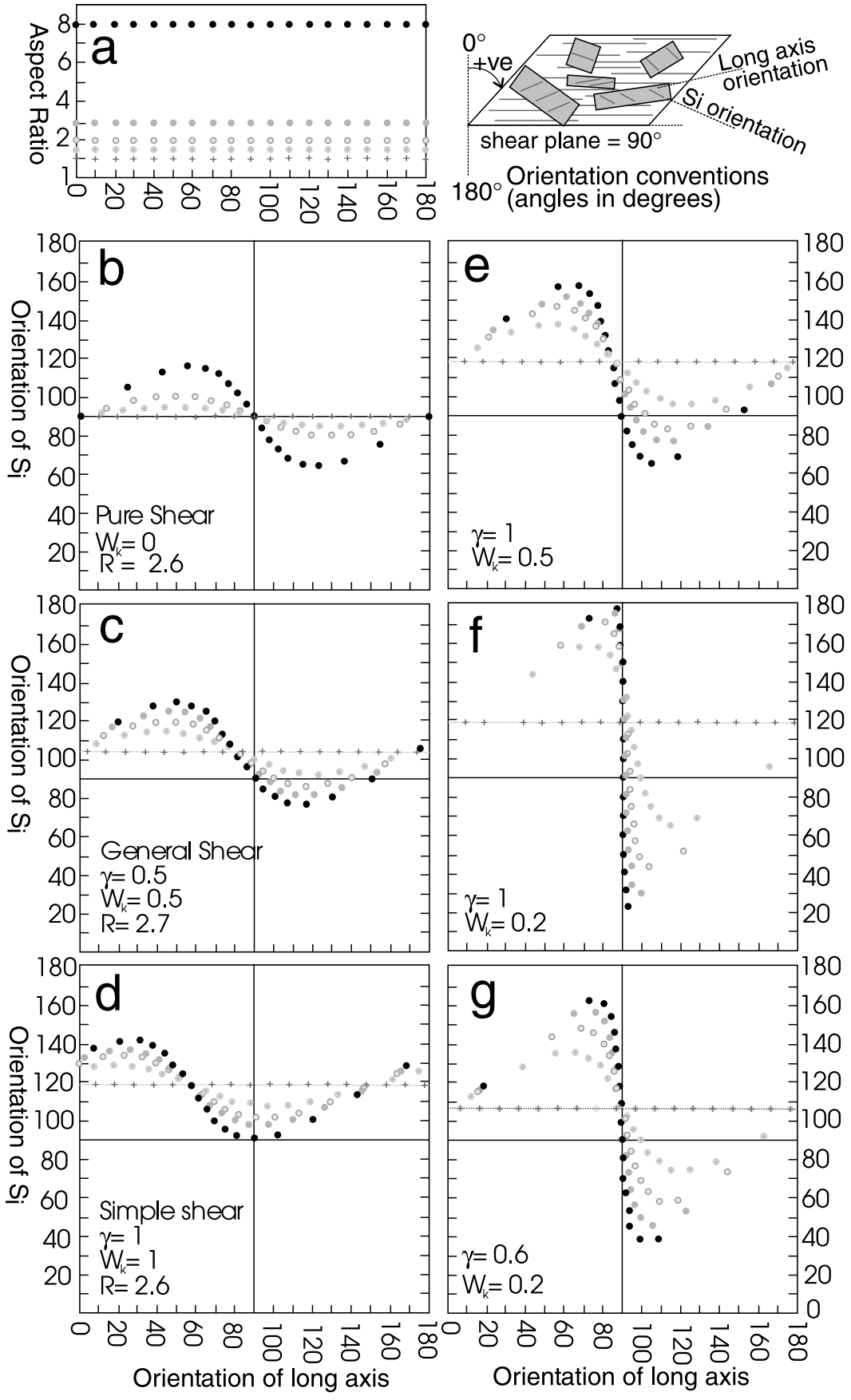
a
Aspect Ratio
0°
+ve
Long axis orientation
Si orientation
shear plane = 90°
180°
Orientation conventions (angles in degrees)
b
Pure Shear
W_k= 0
R= 2.6
e
γ= 1
W_k= 0.5
c
General Shear
γ= 0.5
W_k= 0.5
R= 2.7
f
γ= 1
W_k= 0.2
d
Simple shear
γ= 1
W_k= 1
R= 2.6
g
γ= 0.6
W_k= 0.2
Orientation of Si
Orientation of long axis

axis and the 'peakedness' is a function of γ (Fig. 3d). For all non-pure shear flow regimes, the curves are asymmetrically displaced with respect to the centre of the plot (Fig. 3c–f) and for general flow the 'peakedness' of the curves is a function of both W_k and γ.

All equant porphyroblasts undergo identical rotations, equal to half the bulk shear strain (γ). Thus, all equant objects lie on a line perpendicular to the S_i axis in LA/S_i plots, and the intersection of that line with the S_i axis is a function of the bulk shear strain (the angular difference, in radians, between S_i and the shear plane orientation $= \gamma/2$). Thus, although broadly similar patterns of curves can be generated from different combinations of γ and W_k, the ordinate value of the horizontal line containing equant porphyroblasts fixes the value of the bulk shear strain, and, hence, the remaining shape aspects of the curves ('peakedness', inflection points, minima) are solely a function of W_k (Fig. 3e and f).

The shapes and the patterns of the various distribution curves for different aspect ratios are sensitive to changes in both γ and W_k (Fig. 3), particularly at low-to-moderate values of γ. At high bulk shear strains, low aspect ratio grains can rotate through the shear plane and, hence, the curves start to flow into other quadrants of the plot. It is unlikely that bulk shear or vorticity number could be derived from such data. The curves are very sensitive to changes in the kinematic parameters at moderately low vorticity numbers ($\leqslant 0.6$). Under such conditions, small fluctuations in W_k reflect large changes in the accumulated strain and, hence, the distribution patterns can vary dramatically.

In practice, LA/S_i plots of real data are analysed by comparison with computer generated distributions (Holcombe, 1999). Recognition of a particular type of distribution pattern generally does not require a complete distribution to be present; certain sensitive aspects of the distribution will suffice. Such critical aspects include the horizontal line-containing equant objects (which fix γ), and either the inflection slope of the curve containing high aspect ratio objects, or the extreme S_i values of these objects to fix W_k.

3. Application to the Alpine Schist

3.1. Structure and fabrics

The Alpine Schist near the Franz Josef Glacier on South Island, New Zealand, is a sequence of amphibolite-facies and lower grade graphitic metasiltstone, with subordinate metagreywacke and metavolcanic units (Fig. 1). The structural section is tilted to the southeast and metamorphic grade decreases away from the Alpine Fault from garnet-oligoclase zone in the amphibolite facies to lower greenschist facies near the Main Divide of the Southern Alps about 12 km to the east (Grapes, 1995).

The Alpine mylonite zone lies within ~1 km of the trace of the Alpine Fault and is not exposed in bedrock near the Franz Josef Glacier. Related, lower-strain, non-coaxial ductile fabrics are well exposed just outside the mylonite zone (the so-called 'curly schists'). The well-laminated fabric in these sheared rocks (here called S_4), constitutes the youngest metamorphic foliation in the Alpine Schist, and is clearly related to late Cenozoic slip on the Alpine Fault (Sibson et al., 1981). Their dextral-reverse bulk shear fabrics are approximately parallel to north-east-pitching brittle slip lineations that have been measured locally on the Alpine Fault plane (e.g., Norris and Cooper, 1997). We believe that the mostly weakly lineated, S-tectonite nature of fabrics in these rocks reflects a bulk transpressional flow in the mylonite zone associated with an oblate finite strain (see also Holm et al., 1989).

Within about 1 km of the present trace of the active Alpine Fault near the Franz Josef Glacier on South Island, New Zealand, the youngest ductile fabrics (D_4) broadly reflect the orientation and known kinematics of the fault (dextral with a slight reverse component). These uplifted ductile fault zone rocks are related to late Cenozoic slip on the Alpine Fault (Norris et al., 1990). Their strong S-tectonite fabrics reflect the strongly oblate finite strains in these rocks (Holm et al., 1989). More than ~2 km east of the the Alpine Fault, the D_4 fabric is no longer pervasive, and the structure is dominated by folds of an intensely lineated, older transposition fabric (S_2). These F_3 folds range in size from mm-scale-crenulations to km-scale-inclined folds.

The macroscopic F_3 folds are strongly asymmetric, with structurally inverted short limbs. Fabrics in the hinges and long limbs of the macroscopic folds (and in local parasitic folds) are dominated by a strongly developed crenulation foliation (S_3). In the short limb zones, the S_2 transposition fabric is strongly planar with only sparse F_3 crenulations. F_3 fold axes and the S_2/S_3 intersection lineation are generally colinear with an inherited lineation on the S_2 transposition foliation. Consequently, the rocks are strong LS-tectonites with a shallow-to-moderate, southwest-pitching lineation. Previous workers (Findlay, 1987; Holm et al., 1989) interpreted these planar zones as high strain zones related to the final pre-mylonitic deformation in the Alpine Schist. Our work has shown that the difference between

Fig. 3. Long axis versus S_i plots for different combinations of bulk shear strain (γ) and kinematic vorticity number (W_k). (a) Initial orientation distribution for the specific aspect ratios (varying greyscale), and the orientation conventions used are shown in the plots. (b–d) Plots for a constant finite strain (ellipticity, R, ~2.6) produced by pure shear, general shear, and simple shear respectively. Note that the S_i value of the line containing equant objects (aspect ratio 1) is a function of the shear strain. (d–f) Plots with varying kinematic vorticity number at constant bulk shear strain (see text). (g) Curves thought to be typical of the orientation distribution of biotite in the area described at Franz Josef.

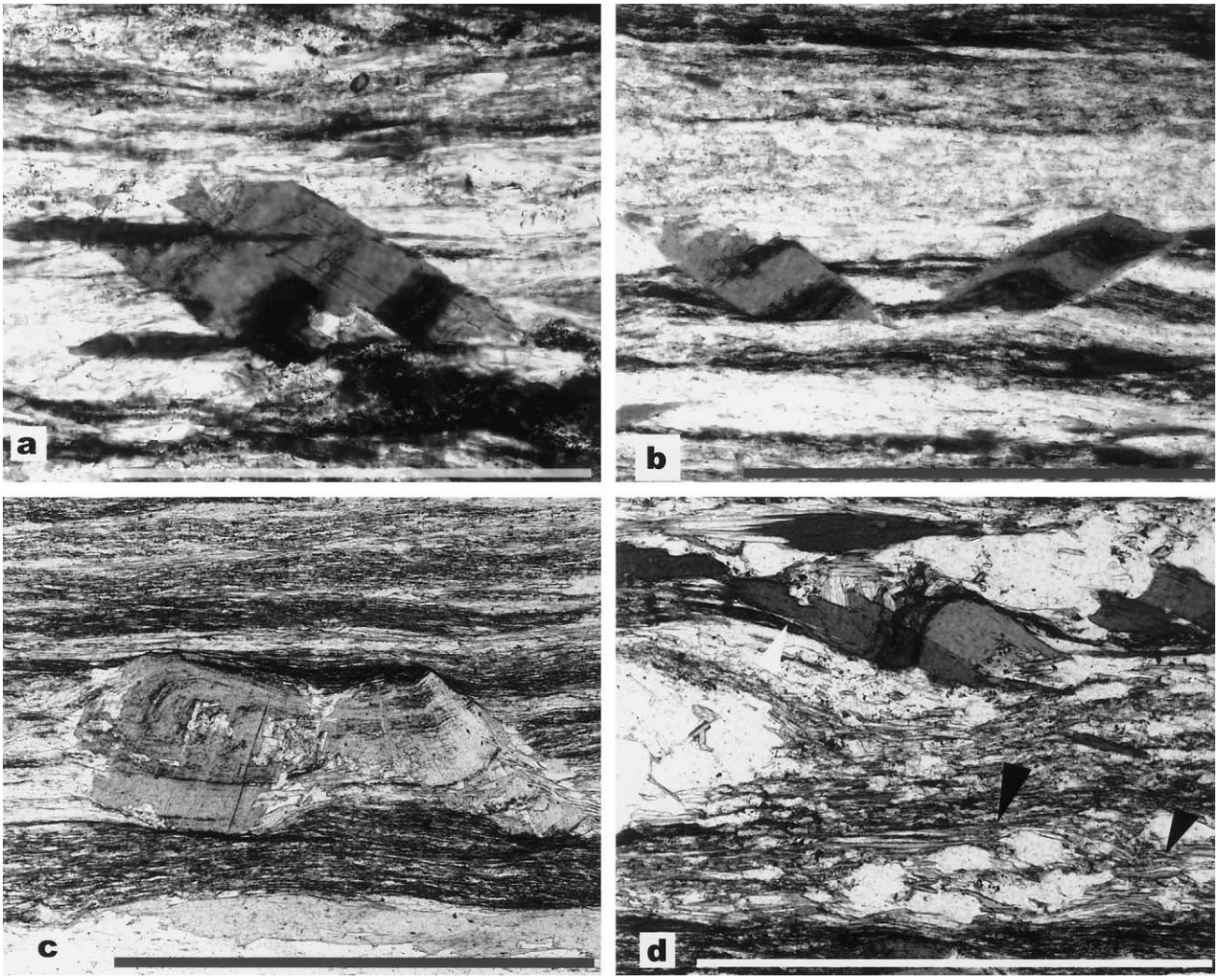

Fig. 4. Biotite porphyroblast microstructures in the planar zone of the Alpine Schist. (a) Bookshelf sliding of microfaulted grains with new biotite grains overgrowing the faults (thin, dark, horizontal grains). New biotite also forms in the asymmetric strain shadow areas. Note that compound grains such as this, while useful for a sense of shear indications, were avoided in the vorticity analysis. (b) Prismatic biotite grains of the type measured in the vorticity analysis. The presence of counter-rotated grains such as that on the right confirm the strong pure shear component of D_{3b} (see text). Microfaults along the grain margin accommodate the rotation, and the displacement can be used to independently calculate the rotation. Note the correlation possible between the internal laminae and the matrix laminae. (c) Prismatic biotite overgrowing relict F_3 crenulation. Such crenulations have been largely obliterated by the D_{3b} deformation in the planar zone fabrics. Such relationships indicate that D_{3b} overprints active D_{3a} crenulation. (d) Shear band fabrics (black arrows) associated with shear along S_2 and a prismatic biotite grain, that has overgrown a D_{3a} crenulation, internally deformed (bending shown by white arrow) by the same shear. Such relationships confirm the shear component of D_{3b}. The length of the scale bar in each photograph is 1 mm. S_2 is horizontal, and the observed consistent sense of shear is to the left (down-dip).

planar and folded zones reflects the position in different limbs of asymmetric folds, and the subsequent dominance of either S_2 or S_3 fabrics.

Abundant porphyroblasts associated with peak metamorphic assemblages (particularly biotite and garnet), accompany the F_3 crenulation foliation (Fig. 4). Biotite shows evidence of syntectonic growth both at the onset, during, and following development of the S_3 crenulation fabric. In the crenulated F_3 hinge zones, large, early prismatic biotite laths (with biotite-filled strain fringes) contain straight inclusion trails of the externally crenulated S_2 fabric, whereas small triangular biotite grains fill dilation sites in the polygonal white mica arcs of S_3 crenulations. In the planar limb zones, variably oriented large prismatic biotite laths overgrow both the graphitic S_2 transposition laminations as well as isolated S_3 crenulations. Such laths are commonly deformed. Grains with (0 0 1) at a high angle to the layering are commonly extended (Fig. 4c), and oblique laths have undergone rotation, microfaulting, and bookshelf sliding (Fig. 4a and b). New biotite growth accompanies this deformation: biotite-filled strain fringes and microboudinage dilation fractures are common; and new biotite laths 'stitch' the microfaults associated with bookshelf sliding packets (Fig. 4a). Many of the large laths containing relict F_3 crenulations have no associated crenulation, preserved within the external fabric (Fig. 4c

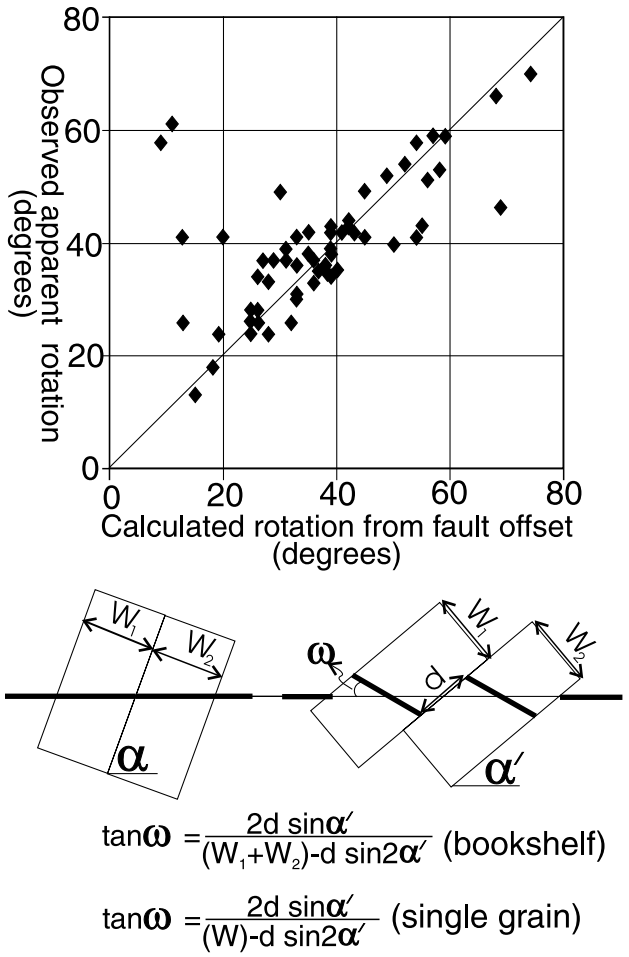

Fig. 5. Correlation plot of the observed apparent rotation angle of biotite grains versus the rotation calculated from microfault offsets using the relationship shown. No. of data = 61, with data compiled from all the thin sections used in this study. Both single isolated grains with clear faulted margins and bookshelf-rotated microfaulted grains were used. Except for ~7 grains, the correlation is very good implying that these grains have indeed achieved their final orientation by rigid body rotation. The discrepant grains most likely preserve crenulation relicts.

and d), indicating that growth of such laths postdated active formation of the crenulation fabric, but the rock has been affected by subsequent strain. This overprinting deformation was associated with decrenulation of the external fabric, which was undergoing layer-parallel extension.

We define the phase of ductile deformation accompanying crenulation as D_{3a}, and that post-dating the formation of active crenulations as D_{3b}. The remainder of this discussion concerns the analysis of D_{3b} coaxiality, bulk shear and vorticity in the planar zones, drawing on aspects of such data to investigate the applicability of the vorticity gauge presented.

3.2. D_{3b} strain and shear sense estimates in the planar fabric zone

The D_{3b} deformation in the planar fabric zones is characterised by a strong component of oblate coaxial deformation across the inherited S_2 layering. Strain fringes around porphyroblasts are aligned along S_2, while a marked decrease in the spacing between graphitic laminae in the matrix relative to their preserved relicts within porphyroblasts (Figs. 4b,d and 5) indicates attenuation of the fabric. Although the large prismatic biotite laths have widely varying orientations, those presently oriented at moderate angles to the layering show both positive and negative rotation sense, dependent on their orientation relative to the layering (Fig. 4b). This behaviour, affecting grains that were initially oriented at quite high angles to the layering (such as those illustrated) indicates a strong coaxial component to the flow. Oblate finite strain is indicated by chocolate-tablet boudinage fractures infilled with biotite, and constant aspect ratio strain shadows in S_2-normal thin sections of all orientations.

Post-peak metamorphic layer-normal shortenings of 25–50% are recorded by the internal/external widths between graphitic laminae (Little and Holcombe, 1998a,b), consistent with shortening of ~50% recorded by buckled quartz veins (Holm et al., 1989). Oblate layer-parallel stretches of ~2 have been estimated using the aspect ratios of strain shadows around garnet and ilmenite porphyroblasts (Little and Holcombe, 1998a,b). The data from these two sets of stretch data are only compatible for three-dimensional (3-D) strain estimates at volume increases of ~100%. Under constant volume assumptions, the bulk 3-D strain estimates derived from two separate types of stretch data are ~1.4:1.4:0.5 (using the shortening data only) or ~2:2:0.25 (using the layer-parallel stretch values only).

A small but consistent component of S_2-parallel shear accompanies the coaxial flattening component in the planar fabric zones. Although prismatic biotite laths have widely varying initial orientations (as shown by the orientation of relict internal layering relative to the long axis), those initially oriented at very high angles to the S_2 layering are consistently rotated in the same sense in any one thin-section. Similar shear sense is indicated by apparent rotation senses of garnet inclusion trails; asymmetric strain shadows around garnet, ilmenite, and biotite porphyroblasts (Fig. 4d); minor shear bands (Fig. 4d), and consistent obliquity of sparse quartz subgrain shape fabrics (Little and Holcombe, 1998a,b).

The strong lineation inherited from the S_2 fabric (and its colinearity with the F_3 folds) complicates recognition of the precise instantaneous shear direction. Thin sections that contain the strongest shear fabrics, or maximum rotations of sub-equant porphyroblasts, tend to pitch steeply down-dip, irrespective of the pitch of the strong inherited L_2 rodding lineation. These observations suggest a dip-slip bulk shear component.

3.3. Shear and vorticity estimates

The large biotite laths in the planar limb zones have

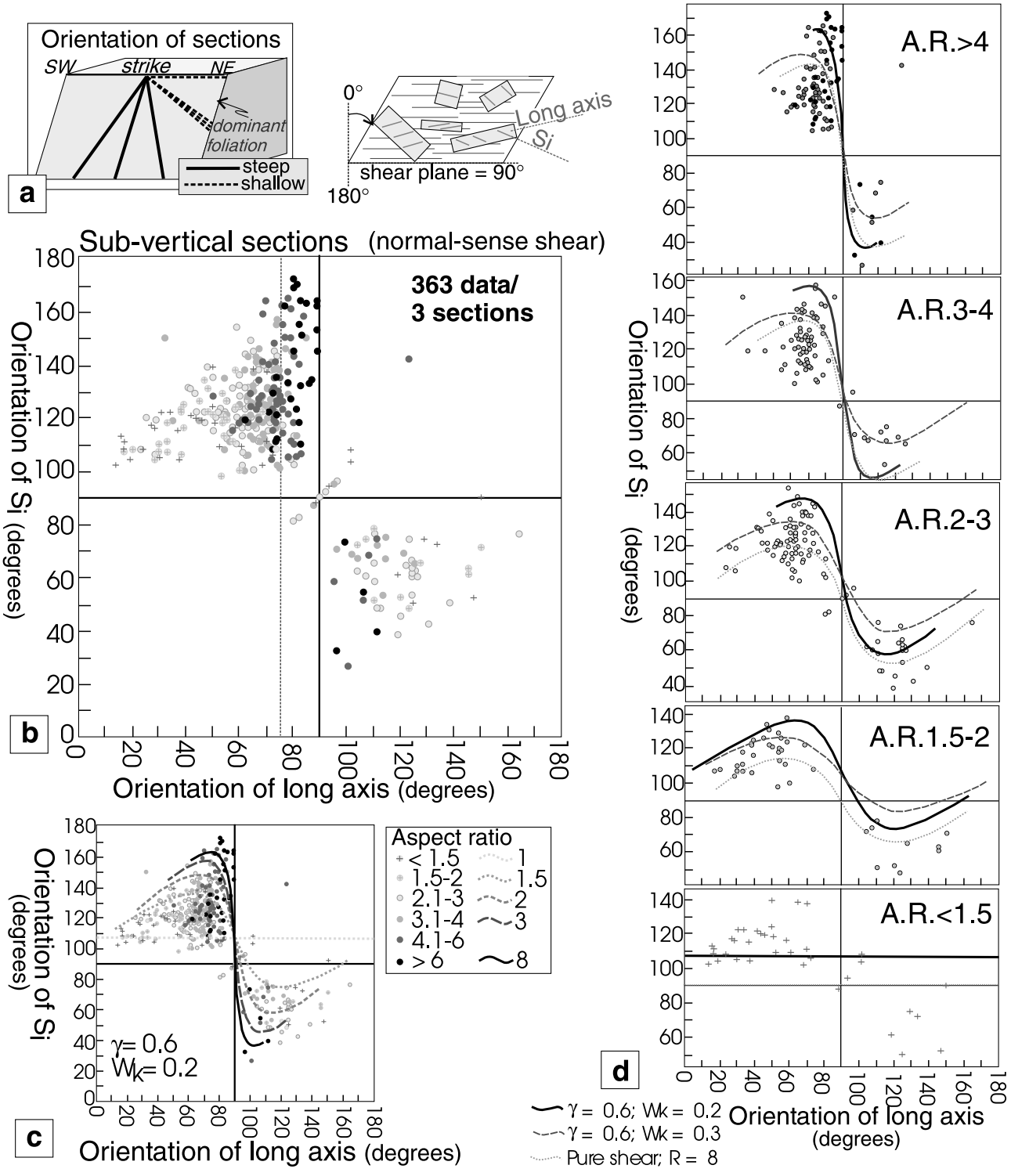

Fig. 6. Long axis versus S_i plots for biotite grains in the Franz Josef area. (a) Orientation of thin sections relative to the dominant planar foliation used in the vorticity plots. All sections are normal to the foliation. Solid lines show the orientations (down-dip) of the sub-vertical sections showing maximum shear fabrics. Dashed lines comprise the orientation of the 'shallow' data set shown in Fig. 8. (b) Plot of 363 biotite grains from locations *b*, *c* and *d* in Fig. 1. The vertical dashed line marks the orientation of the local S_3 crenulation in these sections. (c) Best-fit curves overlain on distribution; (d) individual aspect ratio bands from the distribution shown in (b), with the closest pure shear curve, and curves overlain for $W_k = 0.2$ and $W_k = 0.3$ at a shear strain of 0.6.

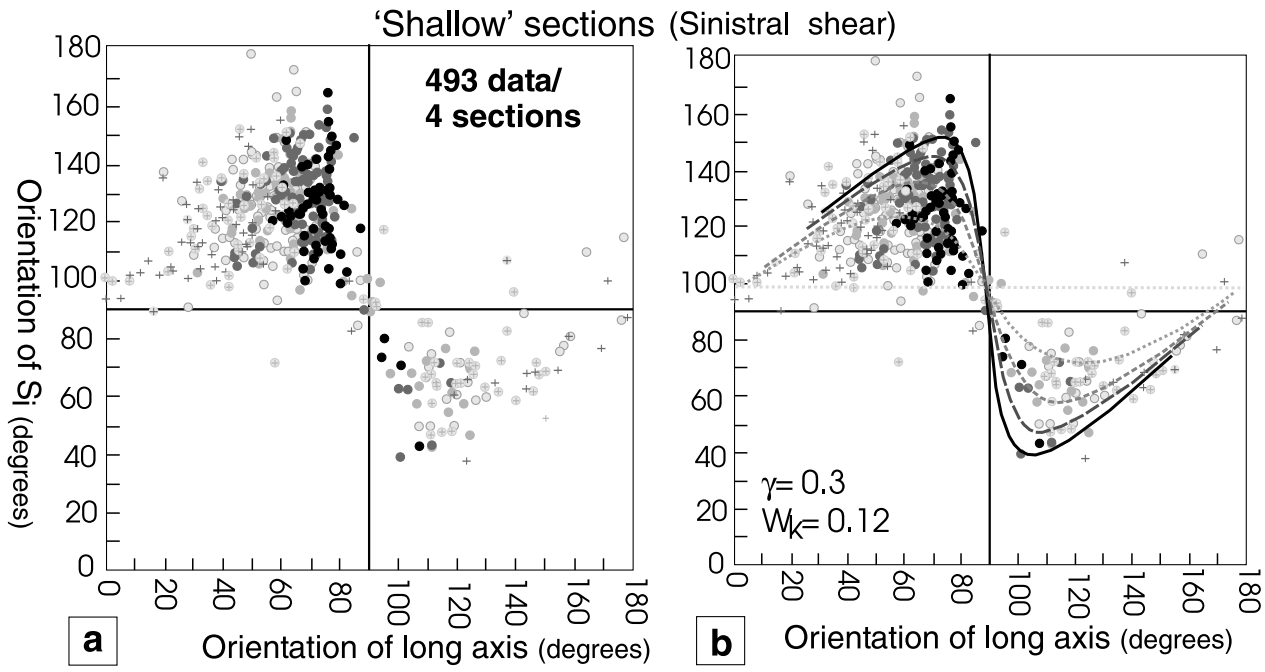

Fig. 7. (a) Long axis versus S_i distributions for shallowly dipping sections from locations *a*, *b*, *d* and *e* in Fig. 1; (b) with best fit curves superimposed. The plots show a slight but significant component of (sinistral) shear indicating that the actual shear direction must have a slight hade in the northeast quadrant rather than being perfectly down-dip.

widely varying aspect ratios and orientations, but laths with the same orientation sense as the local S_3 crenulation dominate. The preservation of the external graphitic laminations as trails within the porphyroblasts, the clear correlation of the two, and the operation of continued shear along the layering provide a good basis for vorticity analysis using the method described above.

The question arises as to whether the S_i relicts within the porphyroblasts are a product of porphyroblast rotation, or of crenulation overgrowth. Certainly, a number of grains exhibit clear evidence of having overgrown crenulations (Fig. 4c and d), and only those with straight S_i inclusion trails are considered in the analysis. Of these, those with a long axis orientation opposed to the S_3 sense consistently show an apparent counter-rotation (as in the right-hand lath in Fig. 4b). If crenulation overgrowth was a major factor in producing the S_i orientation, then such observations would require a further, unrecognised, crenulation fabric in that general orientation. Microfaulting, either at the margins of single grains, or between bookshelf sliding packets, accommodates the apparent rotation on many of these grains. The ability to correlate relict graphitic laminae within porphyroblasts with their matrix parent means that the actual slip in the plane of section on such microfaults can be measured. There is a close linear correlation between the rotation predicted from the slip on such microfaults and the measured apparent rigid body rotation based on the S_i orientation (Fig. 5). Thus, we proceed with some confidence that at least a large component of the isolated laths have undergone rigid body rotation during deformation.

Fig. 6 shows the orientation distribution of 363 large prismatic biotite laths from three separate thin sections each oriented normal to the S_2 layering and pitching approximately down-dip (that is, in the inferred shear direction). All isolated large prismatic biotite porphyroblasts in each section were selected for orientation and shape measurement. Biotite laths that had undergone bookshelf sliding or strong internal deformation were ignored, as were laths that had clearly overgrown crenulations. Although there is considerable noise in the data, the best-fit set of curves to the plot of S_i versus long axes have shear (normal-sense) and vorticity number parameters of $\gamma = \sim 0.6$ and $W_k = 0.2$–0.3.

Fig. 7 shows the orientation distribution of 493 grains from a set of shallowly dipping sections normal to the layering. (The orientation of these sections is shown in Fig. 6a.) The distribution is consistent with a very strong irrotational flattening and a slight component of apparent sinistral shear (in this section) with shear and vorticity values of $\gamma = \sim 0.3$ and $W_k = \sim 0.12$. The shear component in these planes suggests that the bulk shear direction is not strictly dip-slip. Numerous asymmetric microstructures and mesoscopic kinematic indicators specify a dominance of oblique dextral-normal shear in these rocks.

4. Discussion

The presence of a major pure shear component implied from the very low vorticity number estimate is consistent

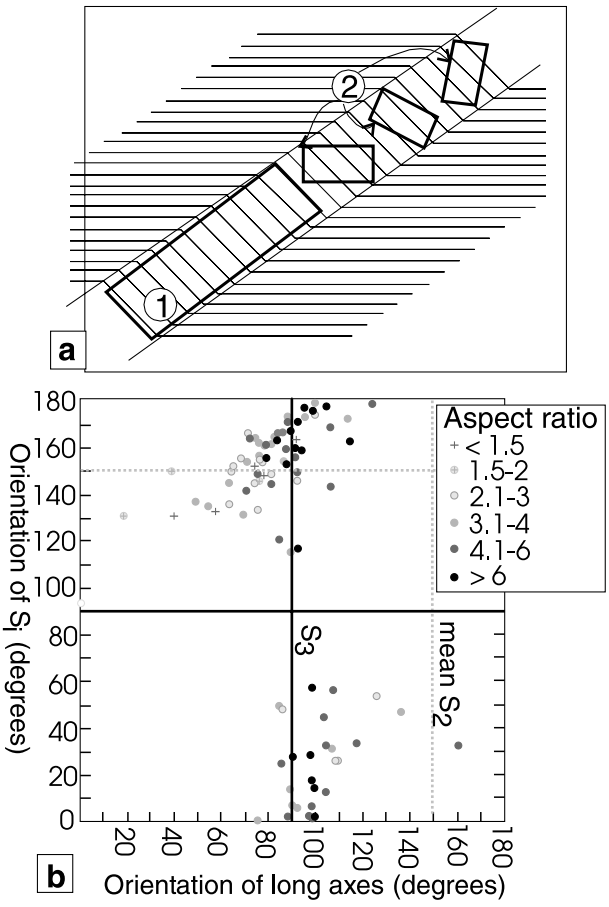

Fig. 8. Relict crenulation control on orientation of biotite lath long axes and thus on long axis versus S_i plots. (a) Theoretical relationships of long and short aspect ratio grains growing within a crenulation; (b) long axis versus S_i plot of 92 biotite laths from a section dominated by F_3 crenulations (location *f* in Fig. 1). High aspect ratio grains (1) tend to be constrained by the crenulation leading to an abnormal concentration of the long axes of such grains parallel to the local S_3 orientation. Small grains of low aspect ratio will tend to be more randomly oriented and hence show an abnormal distribution. In the real data, such lower aspect ratio grains are somewhat controlled by the mean orientation of the crenulated S_2 fabric (dashed line).

with the microstructural observations. The 'noise' in the plots from these data can arise from a number of sources, including shape modification during deformation by dissolution or precipitation processes, or non-ideal behaviour caused by interference and interaction of porphyroblasts during deformation (e.g. Tikoff and Teyssier, 1994). A more important consideration in rocks with multi-deformational histories, such as the Alpine Schist, is the effect of not recognising laths that have overgrown crenulations (in which the S_i orientation is a result of prior folding rather than rigid rotation of the porphyroblast). The effect of such crenulation overgrowth are shown in Fig. 8. The long axes of high aspect ratio grains would be abnormally clustered in a band parallel to the trace angle of the crenulation, and a large degree of S_i noise would be produced in the distribution by low aspect ratio grains. Relict crenulations are a factor in the Alpine Schist rocks and elements of the distribution indicate that unrecognised overgrowths have been included. In particular, there is an anomalously wide distribution of S_i in the low aspect ratio grains that may be due to this effect.

The vorticity and shear values perhaps allow us to resolve the conflicting bulk strain estimates. If we combine the ~0.6 shear estimate from these data with the two sets of 3-D stretch estimates derived previously, and apply the values to Eq. 16 from the 3-D vorticity calculations of Tikoff and Fossen (1995), then we obtain a semi-independent estimate of vorticity number. The vorticity numbers obtained are ~0.45 using the 1.4:1.4:0.5 estimate, and ~0.24 using the ~2:2:0.25 stretch ratios. The latter, higher strain, estimate is much more compatible with the vorticity analysis than the former, suggesting that the rocks may have undergone post-peak metamorphic oblate flattening of up to 75% maximum shortening.

The ductile flow in the Alpine Schist rocks studied is characterised by sub-simple shear. Analysis of abundant kinematic data for ductile and semi-brittle structures in the Franz Josef Glacier region (in progress) has shown that the shear sense is consistently east-block-down (dextral-normal relative to the current steeply southeast-dipping foliation orientation) and is independent of the position in the F_{3a} folds and apparently overprints those structures. These contrast with the dextral-reverse kinematics of the mylonitic rocks adjacent to the Alpine Fault, although both sets of rocks show similar oblate strains of low kinematic vorticity number flow, and were developed under similar peak metamorphic conditions.

The distinction between D_{3a} and D_{3b} is important as, potentially, tens of millions of years may separate these increments, during which interval metamorphic conditions in the mid-crust of the Pacific Plate may have been relatively unchanging (remaining in the garnet zone). We interpret D_{3b} to be a late Cenozoic (<5 Ma) phase of deformation that was acquired by the Pacific Plate rocks prior to, and during, their bending and tilting across the relatively rigid footwall ramp of the Alpine Fault. This imprint of ductile deformation constructively reinforced a pre-existing steep foliation in the rocks, rather than forming a new one.

This deformation would have pre-dated dextral-reverse translation and uplift of the rocks along the Alpine Fault, a final deformation that resulted in the development of the Alpine mylonite zone, and in localized superposition of the youngest ductile fabric adjacent to that structure (D_4). The observation that widespread normal-sense shear on an old fabric accompanies the uplift and exhumation of these rocks implies that models of transpressional uplift of at least this part of the Southern Alps must incorporate elements of antithetic shear, rotation and reactivation of pre-existing, steep foliations in the hangingwall of the Alpine Schist (Little and Holcombe, 1998a,b).

GHOSHFLOW, a computer program for modelling

theoretical S_i/LA distributions is available from: http://www.earthsciences.uq.edu.au/~rodh/software/

Acknowledgements

RJH acknowledges the support of the Australian Research Council (Grant no. E8515071). We thank Donna Kirkwood and an anonymous reviewer for their helpful and most pertinent comments, and R.J. Norris for helpful criticism in personal discussions.

References

Cooper, A.F., Barriero, B.A., Kimbrough, D.L., Mattinson, J.M., 1987. Lamprophyre dike intrusion and the age of the Alpine fault, New Zealand. Geology 15, 941–944.

Findlay, R.H., 1987. Structure and interpretation of the Alpine Schists in Copland and Cook River Valleys, South Island, New Zealand. New Zealand Journal of Geology and Geophysics 30, 117–138.

Ghosh, S.K., 1987. Measure of non-coaxiality. Journal of Structural Geology 9, 111–113.

Ghosh, S.K., Ramberg, H., 1976. Reorientation of inclusions by combination of pure shear and simple shear. Tectonophysics 34, 1–70.

Grapes, R.H., 1995. Uplift and exhumation of Alpine Schist, Southern Alps, New Zealand: thermobarometric constraints. New Zealand Journal of Geology and Geophysics 38, 525–533.

Grapes, R.H., Watanabe, T., 1992. Metamorphism and uplift of the Alpine schist in the Franz-Josef-Fox Glacier area of the Southern Alps, New Zealand. Journal of Metamorphic Geology 10, 171–180.

Holcombe, R.J., 1999. STRAIN CALCULATOR, GHOSHFLOW: programs to calculate and model strain, shear, and vorticity parameters. Geological Society of Australia Abstracts Series 53, 108–109.

Holm, D.K., Norris, R.J., Craw, D., 1989. Brittle and ductile deformation in a zone of rapid uplift: Central Southern Alps, New Zealand. Tectonics 8, 153–168.

Jiang, D., Williams, P.F., 1998. High-strain zones: a unified model. Journal of Structural Geology 20, 1105–1120.

Lin, S., Jiang, Z., Williams, P.F., 1998. Transpression (or transtension) zones of triclinic symmetry: natural example and theoretical modelling. In: Holdsworth, R.E., Strachan, R.A., Dewey, J.F. (Eds.). Continental Transpression and Transtensional Tectonics. Geological Society of London Special Publication 135, pp. 41–57.

Lister, G.S., Williams, P.F., 1983. The partitioning of deformation in flowing rock masses. Tectonophysics 92, 1–33.

Little, T.A., Holcombe, R.J., 1998a. Ductile fabrics in high grade Alpine Schist, Central Southern Alps, New Zealand: what is their relationship to late Cenozoic processes of transpression and uplift. Geological Society of New Zealand Miscellaneous Publication 101A, 151.

Little, T.A., Holcombe, R.J., 1998b. Ductile Fabrics in Zones of Active Transpression: Mechanism of Uplift of the Alpine Schist, Central South Island, New Zealand. Eos Transactions, AGU 79/45, F904.

Means, W.D., 1994. Rotational quantities in homogeneous flow and the development of small-scale structure. Journal of Structural Geology 16, 437–445.

Norris, R.J., Cooper, A.F., 1995. Origin of small-scale segmentation and transpressional thrusting along the Alpine fault, New Zealand. Geological Society of America Bulletin 107, 231–240.

Norris, R.J., Cooper, A.F., 1997. Erosional control on the structural evolution of a transpressional thrust complex on the Alpine Fault, New Zealand. Journal of Structural Geology 19, 1323–1342.

Norris, R.J., Koons, P.O., Cooper, A.F., 1990. The obliquely convergent plate boundary in the South Island of New Zealand: implications for ancient collision zones. Journal of Structural Geology 12, 715–726.

Passchier, C.W., 1987. Stable positions of rigid objects in non-coaxial flow—a study in vorticity analysis. Journal of Structural Geology 9, 679–690.

Passchier, C.W., Trouw, R.A.J., 1996. Microtectonics. Springer-Verlag, Berlin.

Robin, P.-Y.F., Cruden, A.R., 1994. Strain and vorticity patterns in ideally ductile transpression zones. Journal of Structural Geology 16, 447–466.

Sibson, R.H., White, S.H., Atkinson, B.K., 1981. Structure and distribution of fault rocks in the Alpine Fault Zone, New Zealand. Geological Society of London Special Publication 9, 197–210.

Sutherland, R., 1995. The Australia–Pacific boundary and Cenozoic plate motions in the SW Pacific: some constraints from Geosat data. Tectonics 14, 819–831.

Tikoff, B., Fossen, H., 1995. The limitations of three-dimensional kinematic vorticity analysis. Journal of Structural Geology 17, 1771–1784.

Tikoff, B., Teyssier, C., 1994. Strain and fabric analysis based on porphyroblast interaction. Journal of Structural Geology 16, 477–491.

Walcott, R.I., 1998. Modes of oblique compression: late Cenozoic tectonics of the South Island of New Zealand. Reviews of Geophysics 36, 1–26.

Wellman, H.W., 1979. An uplift map for the South Island of New Zealand, and a model for the uplift of the Southern Alps. Royal Society of New Zealand Bulletin 18, 13–20.